Synthesis, Thermal, DFT Calculations, HOMO-LUMO, MEP, and Molecular Docking Analysis of New Derivatives of Imidazolin-4-Ones

Khedidja Merdja[1,2], Choukry Kamel Bendeddouche[1], Mokhtaria Drissi[2], Farah Chafika Kaouche[2], Nassima Medjahed[3,4], José Manuel Padrón[5], Mansour Debdab[2*], Mustapha Rahmouni[2], and El Habib Belarbi[2]

[1]*Laboratory of Applied Organic Synthesis, Faculty of Exact and Applied Sciences, University Oran1 Ahmed Ben Bella, El M'Naouer, Oran 31000, Algeria*

[2]*Laboratory of Synthesis and Catalysis (LSCT), Faculty of Materials Sciences, University Ibn Khaldoun-Tiaret, Tiaret 14000, Algeria*

[3]*Laboratoire de Catalyse et Synthèse en Chimie Organique, Faculté des Sciences, Université de Tlemcen, Tlemcen 13000, Algeria*

[4]*Faculté des Sciences et de la Technologie, Université d'Ain Témouchent, Ain Témouchent 46000, Algeria*

[5]*BioLab, Instituto Universitario de Bio-Organica "Antonio González", Universidad de La Laguna, La Laguna 38200, Spain*

**** Corresponding author:***

email: mansour.debdab@univ-tiaret.dz

Received: July 29, 2023
Accepted: September 20, 2023

DOI: 10.22146/ijc.87476

Abstract: *This work focuses on synthesizing new imidazolin-4-one derivatives (**2a-c**), akin to leucettamine B analogs, via microwave-assisted transamination reactions. This reaction was carried out between 3-alkyl-5-dimethylamino-2-thioxo-imidazolidin-4-one (**1a-c**) and aniline. The structural integrity of the synthesized compounds was confirmed using NMR and MS spectroscopy, and their configurations were validated through DFT calculations. Analyses encompassed molecular electrostatic potential, frontier molecular orbitals, HOMO-LUMO energies, energy band gap, and global chemical reactivity descriptors, providing comprehensive insights into their characteristics. The investigation extended to the biological domain, employing substance activity spectra prediction (PASS) and molecular docking with Autodock Vina4 program. Notably, this holistic assessment aimed to gauge the potential regulatory effect of the compounds on cholesterol. This integrated approach contributes to compound design understanding and potential applications, spanning drug design and broader biomedical contexts.*

Keywords: *DFT calculations; imidazolin-4-ones derivatives; HOMO-LUMO energies; microwave irradiation; molecular docking*

■ INTRODUCTION

Marine natural products have evolved considerably and have become very interesting sources of inspiration for new drug discovery [1]. Most of the compounds have spurred improvements in organic chemistry, especially in synthesis methodologies, thereby paving the way to synthesize analogs with improved pharmacological or pharmaceutical properties [2-5]. From this point of view, marine sponges provide without a doubt a vast store of unique and physiologically active natural compounds that need to be studied.

The study of 2-thiohydantoin derivatives as well as 2-aminoimidazolin-4-one has attracted the interest of many researchers both in synthesis and in the study of their properties [6-7], particularly as a material first for the preparation of synthetic intermediates with a wide range of applications in several fields as therapeutic agents [8-9] antifungals, herbicides [10-11], antitumors [12], and other biological activities [13]. As a consequence, the development of solvent-free organic synthesis using microwaves has gained much interest [14-15].

The purpose of this study is to synthesize new molecule derivatives of 2-thiohydantoins using aniline as the aromatic amine in the transamination step, and then we conducted *in silico* investigations using DFT calculations, activity prediction, and molecular docking. Chérouvrier et al. [16] used this strategy to obtain analogues of leucettamine B. However, aniline was not used in this reaction.

As far as we know, the transamination of 5-dimethylaminomethylene-3-alkyl-2-thioxoimidazolidin-4-ones (**1a**-**c**) using aniline under microwave irradiation (M.W.I.) has not been described previously. In this framework, we report our first results concerning this strategy for the synthesis of new derivatives of imidazolin-4-ones according to Scheme 1.

It is widely established that in organic frameworks with large delocalized π-systems, π-electrons are more polarizable due to their further enhancement by the donor and acceptor substituents incorporation at the extremities of the conjugated system [17]. The magnitude of the charge transfer is largely determined by these groups at the opposite ends.

The compounds **1a**-**c** and **2a**-**c** were calculated using the density functional theory (DFT) method with B3LYP/6-311G(d,p) basis set. The molecular electrostatic potential (MEP) shape is a plot of electrostatic potential mapped onto the constant electron density surfaces, which provides information about charge density distributions, nucleophilic, and electrophilic reaction sites for hydrogen bonding interactions in a molecule.

The MEP map and the energies (HOMO and LUMO) of the compound were determined using DFT/B3LYP method with 6-311G(d,p) basis set in Gaussian 09 software program. In addition, the prediction of activity spectra for substances (PASS) and molecular docking methods were employed to conduct a comprehensive investigation, yielding essential information for determining the biological activity of the investigated compounds.

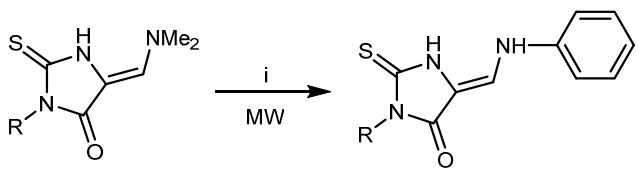

1a-c **2a-c**

Scheme 1. Reagents and conditions: (i) Ph-NH_2 (4 eq), MW, for **2a**: R = Me, 70 °C, 5 min; for **2b**: R = Bu, 70 °C, 5 min for **2c**: R = Ph, 70 °C, 10 min

■ EXPERIMENTAL SECTION

Materials

The reagents used in this study without any further purification are *N*,*N*-dimethylformamide dimethyl acetal 94% (DMF-DMA) and aniline (≥ 99%).

Instrumentation

A Bruker Ascend TM 300 was used to record the ^{1}H-NMR and ^{13}C-NMR spectra at 300 and 75 MHz, respectively. Shifts (δ) are presented in ppm relative to the residual proton signal of DMSO-d_6 at 2.50 ppm (m). A Q-exactive mass spectrometer and electrospray ionization (ESI) were used to record mass spectra. Sample injection (MeOH as solvent) was carried out using UHPLC without a column (50 L and 3 min acquisition at 0.200 mL/min). The acquisition was carried out with a full scan at 60,000 resolutions. The capillary temperature was 350 °C and the source voltage was 3.5 kV. Spectra were recorded in positive mode and calibrated using the Pierce™ LTQ Velos ESI Positive Ion Calibration Solution (Thermo Fisher Scientific). A Kofler melting point apparatus was used to determine the melting points (m.p.) of all products with a temperature reading scale graduated from 50 °C to 260 °C.

Procedure

Synthesis and characterization of 5-dimethylaminomethylene-3-alkyl-2-thioxoimidazolidin-4-ones (1a-c)

5-Dimethylaminomethylene-3-alkyl-2-thioxoimidazolidin-4-ones (**1a**-**c**) were synthesized following procedures described in the literature [16,18]. Briefly, a mixture of 3-alkyl-2-thioxo-imidazolidin-4-one and DMF-DMA (1.2 eq) was reacted in a microwave for 30 min at 70–80 °C. After cooling at room temperature, the crude products were washed with

ethanol. The aminomethylenation products (**1a**-**c**) were obtained as a solid in yields ranging from 74 to 77%.

General method for the synthesis of 3-alkyl-5-phenylaminomethylene-2-thioxoimidazolidin-4-ones (2a-c)

A mixture of 5-dimethylaminomethylene-3-alkyl-2-thioxoimidazolidin-4-one (**1a**-**c**) and aniline (4 eq) was reacted in a microwave at 70 °C for 5 to 10 min (Scheme 2). When the reaction was completed, the crude reaction mixture was allowed to cool down at room temperature, and then ethanol was added until the compounds had completely precipitated. The expected compounds were obtained after filtration on sintered glass.

■ RESULTS AND DISCUSSION

The new imidazolin-4-ones **2a**-**c** were obtained by a simple transamination reaction between 3-alkyl-5-dimethylamino-2-thioxo-imidazolidin-4-ones **1a**-**c** and aniline using the eco-friendly solventless methodology under microwave irradiation. The expected compounds were obtained in good yields ranging from 70 to 84% after filtration and by adding the ethanol. ^{1}H-NMR, ^{13}C-NMR, and mass spectrometry were used to confirm the obtained product structures. The ^{1}H-NMR shows that the reaction is stereospecific. In fact, only one stereoisomer is observed in ^{1}H-NMR of the reaction product. The exocyclic double bond proton C=CH has a chemical shift of about 9 ppm. The coupling constant ^{3}J = 13.2 Hz [19] for compounds **2a** and **2b** that exists between the exocyclic vinyl proton C–H and the amino proton N–H lead to the suggestion of the trans relation between these two hydrogens about the C–N bond which acquires partial double character due to conjugation. However, this vinylic C–H appears as a singlet in the case of **2c** caused by the fast exchange of the proton of the amine group. The appearance of the signals of phenyl and N–H groups at respectively 7.00 and 7.40 ppm (**2b**) affirm the transamination reaction. This result is confirmed by ^{13}C-NMR, which shows the signals of sp^2 carbons of the phenyl group varying from 108 to 138 ppm. Moreover, the comparison between experimental and theoretical ^{1}H- and ^{13}C-NMR spectra obtained by Gaussian 09 confirms the obtaining of imidazolin-4-ones derivatives (**2a**-**c**) (Fig. S9).

NMR and MS Spectroscopies Results

3-Methyl-5-phenylaminomethylene-2-thioxoimidazolidin-4-one (2a)

Yield: 70%; yellow powder; m.p. > 260 °C. ^{1}H-NMR (300 MHz, DMSO-d_6): δ 3.13 (s, 3H, NC**H**$_3$), 7.00 (t, J = 7.3 Hz, 1H, Ar), 7.16–7.19 (m, 2H, Ar), 7.30–7.40 (m, 3H, Ar, NH), 9.09–9.13 (d, J = 13.2 Hz, 1H, C=C**H**), 11.35 (br s, 1H, NH) (Fig. S1). ^{13}C-NMR (75 MHz, DMSO-d_6):

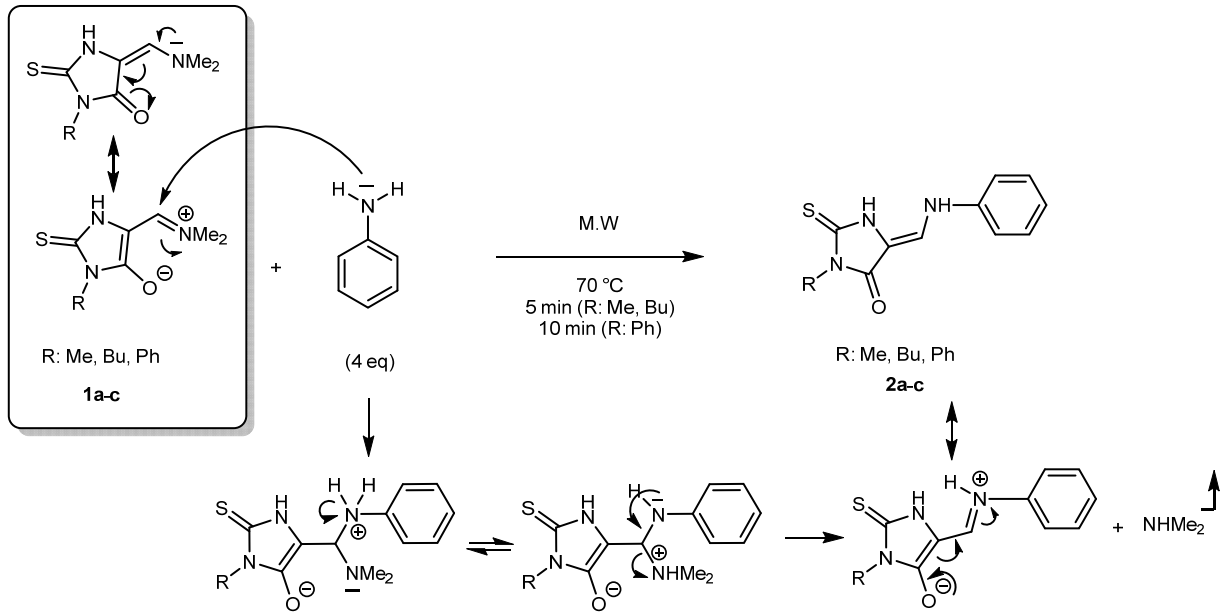

Scheme 2. Synthesis of 3-alkyl-5-phenylaminomethylene-2-thioxoimidazolidin-4-ones (**2a**-**c**) with mechanism

δ 27.33 (N**C**H$_3$), 108.34 (C-Ar), 115.58 (2 C-Ar), 119.13 (NH**C**=CH), 123.01 (C-Ar), 130.17 (2 C-Ar); 140.62 (C=**C**H), 163.18 (C=O), 171.76 (C=S) (Fig. S2). HRMS, *m/z*: 234.0697 found (calculated for $C_{11}H_{12}N_3OS$, $[M + H]^+$ requires: 234.0696) (Fig. S7).

3-Butyl-5-phenylaminomethylene-2-thioxoimidazolidin-4-one (2b)

Yield: 82%; light brown powder; m.p. = 224–226 °C. ^{1}H-NMR (300 MHz, DMSO-d_6): δ 1.06 (t, J = 7.0 Hz, 3H, $NCH_2CH_2CH_2C\mathbf{H}_3$), 3.10–3.17 (m, 4H, $NCH_2C\mathbf{H}_2C\mathbf{H}_2CH_3$), 3.42–3.47 (q, J = 7.0 Hz, 2H, $NC\mathbf{H}_2CH_2CH_2CH_3$), 7.02 (t, J = 7.3 Hz, 1H, Ar), 7.19 (d, J = 8.0 Hz, 2H, Ar), 7.32–7.41 (m, 3H, Ar, NH), 9.10–9.13 (d, J = 13.1 Hz, 1H, C=C**H**), 11.36 (br s, 1H, NH) (Fig. S3). ^{13}C-NMR (75 MHz, DMSO-d_6): δ 19.01 ($NCH_2CH_2CH_2\mathbf{C}H_3$), 27.34 ($NCH_2CH_2\mathbf{C}H_2CH_3$), 39.60 ($NCH_2\mathbf{C}H_2CH_2CH_3$), 56.50 ($N\mathbf{C}H_2CH_2CH_2CH_3$), 108.34 (C-Ar), 115.63 (2 C-Ar), 119.22 (NH**C**=CH), 123.06 (C-Ar), 130.21 (2 C-Ar), 140.64 (C=**C**H), 163.21 (C=O), 171.80 (C=S). (Fig. S4). HRMS, *m/z*: 276.1169 found (calculated for $C_{14}H_{18}N_3OS$, $[M + H]^+$ requires: 276.1165) (Fig. S8).

3-Phenyl-5-phenylaminomethylene-2-thioxoimidazolidin-4-one (2c)

Yield: 84%; dark brown powder; m.p. > 260 °C. ^{1}H-NMR (300 MHz, DMSO-d_6): δ 7.12 (t, J = 7.4 Hz, 1H, Ar), 7.35–7.40 (m, 2H, Ar), 7.48–7.58 (m, 3H, Ar), 7.66–7.70 (m, 4H, Ar), 8.09 (s, 1H, C=C**H**), 9.97 (s, 1H, NH), 13.03 (br s, 1H, NH) (Fig. S5). ^{13}C-NMR (75 MHz, DMSO-d_6): δ 120.22 (NH**C**=CH), 123.17 (C-Ar), 123.86 (C-Ar), 124.35 (C-Ar), 126.44 (2 C-Ar), 128.82 (C-Ar), 129.36 (2 C-Ar), 129.44 (3 C-Ar), 137.78 (C-Ar), 138.87 (C=**C**H), 156.07 (C=O), 164.24 (C=S) (Fig. S6).

Computational Results and Discussion

The Gaussian 09 set of quantum chemistry codes were used to perform the ground state calculations [20]. Gauss View 5 software was used to visualize the output files [21]. The structural properties of compounds **1a**-**c** and **2a**-**c** were determined by applying Becke's three-parameter hybrid functional (B3) for the exchange part and the Lee-Yang-Parr (LYP) correlation function [22] with 6-31G(d,p) level in order to obtain the optimized geometrical parameters of the compound. The MEP and HOMO–LUMO energies were calculated at the same level. Additionally, the global reactivity descriptors and the dipole moment are also calculated to understand the reactive nature of the compound. For a more in-depth study to provide additional information as a basis for determining the biological activity of the studied compounds, we used PASS and the molecular docking method using Autodock Vina4 [23].

We harnessed Autodock Vina4 for conducting molecular docking and leveraged the Pass Online tool to predict the biological activity of the identified compounds namely, **lig1** (**2a**), **lig2** (**2b**), and **lig3** (**2c**). Our discerned results substantiate the potential of these compounds to function as enhancers of HMGCS2 expression. Employing molecular docking, we delved into the preferred orientations and binding mechanisms of these molecules within HMGCS2's active site. This comprehensive exploration facilitates insights into intricate molecular interactions, encompassing hydrogen bonding, hydrophobic interactions, and electrostatic forces. These interactions collectively underscore the fundamental stabilizing factors governing the system's integrity.

Frontier molecular orbital's (FMOs) studies: Global reactivity descriptors

The charge transfer placed within the molecule was explained by analyzing the HOMO and LUMO. Both orbitals named as FMOs. The FMOs energies (E_{HOMO}, E_{LUMO}) were employed to determine the global chemical reactivity descriptors of the molecule such as the ionization potential electron affinity, the electronegativity, the global hardness, the global softness, the chemical potential, and the electrophilicity index [24-25]. Two important molecular properties, electronegativity and hardness, are useful for interpreting and understanding the stability and reactivity of molecular systems [26].

The HOMO-LUMO energy gap explains the concluding charge transfer interaction within the molecule and is useful in determining molecular electrical transport properties. A molecule with a small frontier orbital gap (HOMO-LUMO energy gap) has high chemical reactivity and low kinetic stability [27-29]

because it is energetically favorable to add an electron to the high-lying LUMO in order to remove electrons from the low-lying HOMO. Therefore, HOMO-LUMO energies are used to determine different chemical properties such as the global reactivity descriptors (ΔE), ionization potential (IP = $-E_{HOMO}$), electron affinity (EA = $-E_{LUMO}$), global chemical hardness (η = (IP−EA)/2), global chemical softness (s = 1/2η), electronegativity (χ = (IP+EA)/2), chemical potential (μ = −(IP+EA)/2) and electrophilicity index (ω = $\mu^2/2\eta$).

The HOMO-LUMO gap energy and the dipole moment listed in Table 1 of the title compound were computed with DFT/B3LYP/6-311G(d,p) method. The calculated values of the global reactivity descriptors are also listed in Table 1. The FMO's atomic orbital compositions can be seen in Fig. 1 and 2.

In the group of **2a**-**c**, the best electron donor is compound **2b**, which has the highest HOMO energy (E_{HOMO} = −5.385 eV) and the lowest ionization value (IP = 5.385 eV), while the best electron acceptor is compound **2c**, which has the lowest LUMO energy (E_{LUMO} = −1.673 eV), the highest electron affinity (EA = 1.673 eV), and the highest ionization value (IP = 0.5413 eV) (Table 2). Furthermore, compound **2c** showed the smallest orbital energy gap (ΔE = 3.74 eV) among the investigated products as the consequence of the highest chemical reactivity, least kinetically stable "soft molecule", and the most polarizable form (Fig. 2). The reactivity of these compounds is the greatest based on energy gap (ΔE) parameters, which support that compound **2a** is the most stable as compared to others as follow the order **2a** > **2b** > **2c** (Fig. 2). It is important

Table 1. Some quantum chemical molecular descriptors computed of the **1a**-**c** compounds using DFT/B3LYP/6-311G(d,p)

Compounds	Compound **1a**	Compound **1b**	Compound **1c**
E_{HOMO} (eV)	−5.277	−5.252	−5.279
E_{LUMO} (eV)	−1.281	−1.265	−1.321
$\|E_{HOMO}-E_{LUMO}\|$ (eV)	3.996	3.987	3.957
Dipole moment μ (Debye)	6.784	6.584	6.741
IP (eV)	5.277	5.252	5.279
EA (eV)	1.281	1.265	1.321
η (eV)	1.998	1.993	1.979
S (eV^{-1})	0.250	0.251	0.253
χ (eV)	3.279	3.258	3.300
μ (eV)	−3.279	−3.258	−3.300
ω (eV)	2.690	2.662	2.753

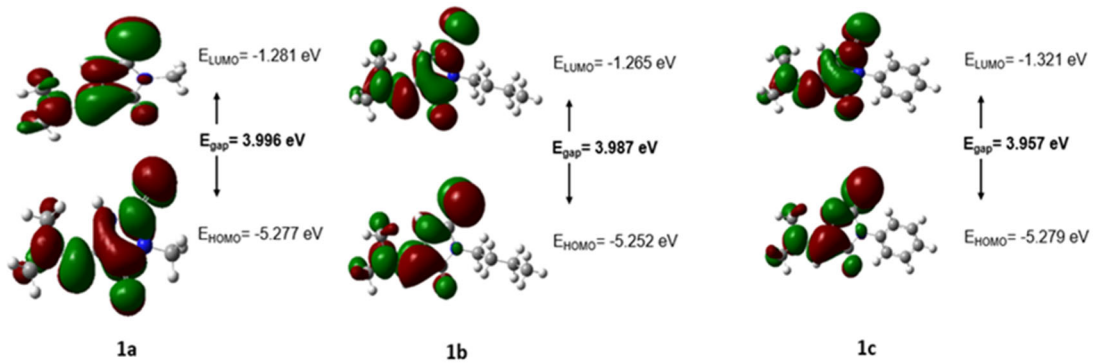

Fig 1. The molecular orbitals and energies for the HOMO and LUMO with the numbering of atoms for the 5-dimethylaminomethylene-3-alkyl-2-thioxoimidazolidin-4-ones (**1a-c**)

Table 2. Some computed quantum chemical molecular descriptors of the **2a**-**c** compounds using DFT/B3LYP/6-311G(d,p)

Compounds	Compound **2a**	Compound **2b**	Compound **2c**
E_{HOMO} eV	−5.423	−5.385	−5.413
E_{LUMO} eV	−1.645	−1.626	−1.673
$\|E_{HOMO}-E_{LUMO}\|$ (eV)	3.777	3.758	3.740
Dipole moment μ (Debye)	5.783	5.577	5.668
IP (eV)	5.423	5.385	5.413
EA (eV)	1.645	1.626	1.673
η (eV)	1.889	1.879	1.870
S (eV^{-1})	0.265	0.266	0.267
χ (eV)	3.534	3.505	3.543
μ (eV)	−3.534	−3.505	−3.543
ω (eV)	3.305	3.268	3.356

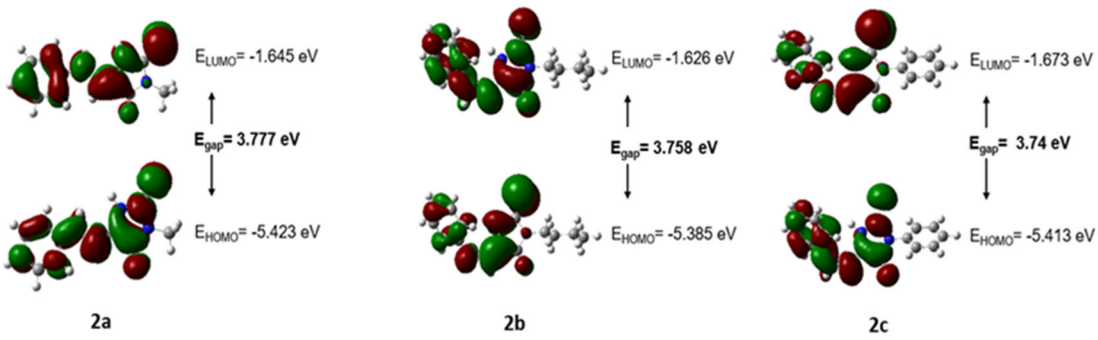

Fig 2. The molecular orbitals and energies for the HOMO and LUMO with the numbering of atoms for the titles compounds3-alkyl-5-phenylaminomethylene-2-thioxoimidazolidin-4-one (**2a**-**c**)

to measure other important parameters such as η, S, and μ to measure the stability of the compound.

Mulliken population analysis

Quantifying the electronic structure changes caused by atomic displacements can be done by using atomic charge calculations, which can be used to explain changes in molecular properties. The Mulliken [30] population analysis is the most widely known of all models for predicting individual atomic charges, and it is highly computationally popular due to its simplicity. It was observed that Mulliken charges are highly dependent on basis sets and unpredictable, with significant fluctuations in partial charges [31].

The atomic charge values calculated by Mulliken analysis for **1a**-**c** and **2a**-**c** at the BPV86 functional with the 6-311G(d,p) basis set are summarized in Table 3 and 4. According to Mulliken results, all of the hydrogen atoms are positively charged. In these molecules, the H_1 and H_3 atoms have high positive Mulliken charges of 0.273 and 0.279 e, respectively. These charges are important compared to the other hydrogen atoms due to the electronegative character of the N_2 and N_3 atoms. The large positive charge values of hydrogen atoms indicate the presence of intra and inter-molecular hydrogen bonding in the crystal packing. On the other hand, the sulfur, oxygen, and nitrogen atoms have the most negative charges in the four title molecules. The carbon atoms bound to the sulfur, oxygen, and nitrogen atoms have positive charges due to their electron-withdrawing nature. The calculated Mulliken charges are in complete agreement with the molecular electrostatic potential results using the BPV86/6-311G(d,p) level of theory.

Table 3. Atomic charges distribution for 5-dimethylaminomethylene-3-alkyl-2-thioxoimidazolidin-4-ones (**1a**-**c**) calculated by Mulliken method using the BPV86/6-311G(d,p) level in the gas phase

Compound **1a**		Compound **1b**		Compound **1c**	
1C	0.553	1C	0.555	1C	0.556
2C	0.214	2C	0.272	2C	0.275
3C	0.360	3C	0.360	3C	0.362
4N	−0.498	4N	−0.499	4N	−0.509
5S	−0.288	5S	−0.270	5S	−0.271
6N	−0.631	6N	−0.624	6N	−0.626
7C	0.121	7C	0.077	7C	0.077
8H	0.140	8H	0.145	8H	0.145
9N	−0.422	9N	−0.606	9N	−0.607
10C	−0.176	10C	−0.176	10C	-0.176
10HA	0.126	10HA	0.126	10HA	0.126
10HB	0.125	10HB	0.125	10HB	0.125
10HC	0.136	10HC	0.136	10HC	0.136
11C	−0.190	11C	0.289	11C	−0.190
11HA	0.138	11HA	0.138	11HA	0.138
11HB	0.127	11HB	0.127	11HB	0.127
11HC	0.130	11HC	0.130	11HC	0.130
12H	0.273	12H	0.273	12H	0.273
13O	−0.527	13O	−0.527	13O	−0.527
14C	−0.176	14C	−0.050	14C	0.264
14HA	0.144	14HA	0.113	15C	-0.081
14HB	0.145	14HB	0.134	15HA	0.104
14HC	0.146	15C	−0.176	16C	−0.104
		15HA	0.118	16HA	0.081
		15HB	0.108	17C	-0.074
		16C	−0.178	17HA	0.085
		16HA	0.100	18C	−0.103
		16HB	0.096	18HA	0.090
		17C	−0.319	19C	−0.064
		17HA	0.107	19HA	0.110
		17HB	0.104		
		17HB	0.100		

Table 4. Atomic charges distribution for and3-alkyl-5-phenylaminomethylene-2-thioxoimidazolidin-4-ones (**2a**-**c**) calculated by Mulliken method using the BPV86/6-311G(d,p) level in the gas phase

Compound **2a**		Compound **2b**		Compound **2c**	
1C	0.555	1C	0.556	1C	0.553
2C	0.272	2C	0.275	2C	0.273
3C	0.360	3C	0.362	3C	0.359
4N	−0.499	4N	−0.509	4N	−0.613
5S	−0.270	5S	−0.271	5S	−0.255
6N	−0.624	6N	−0.626	6N	−0.523
7C	0.077	7C	0.077	7C	0.078
8H	0.145	8H	0.145	8H	0.146
9N	−0.606	9N	−0.607	9N	−0.606
11C	0.289	11C	0.289	11C	0.289
24C	−0.176	24C	−0.050	15O	−0.508
24HA	0.146	24HA	0.139	10H	0.276
24HB	0.147	24HB	0.130	12C	−0.139
24HC	0.148	15O	−0.525	13C	−0.113
14H	0.286	10H	0.276	14C	−0.091
15O	−0.519	12C	−0.139	15H	0.119
10H	0.270	13C	−0.113	16C	−0.088
12C	−0.139	14C	−0.091	17H	0.089
13C	−0.113	15H	0.119	18C	−0.083
14C	−0.091	16C	−0.088	19H	0.105
15H	0.119	17H	0.089	20H	0.098
16C	−0.088	18C	−0.083	21H	0.096
17H	0.089	19H	0.105	24C	0.261
18C	−0.083	20H	0.098	25C	−0.052
19H	0.105	21H	0.096	26C	−0.061
20H	0.098	27C	−0.175	27C	−0.103
21H	0.096	28H	0.108	28H	0.110
		29H	0.118	29C	−0.103
		30C	−0.179	30H	0.103
		31H	0.100	31C	−0.073
		32H	0.096	32H	0.091
		33C	−0.319	33H	0.090
		34H	0.101	34H	0.087
		35H	0.104		

Molecular electrostatic potential

Generally, the electrophilic and nucleophilic sites of a molecule can be located by studying electrostatic potential (ESP) [32]. It is a valuable and useful tool for molecular modeling studies. Predicting the interaction between different geometries can be done easily using the MEP contour map [33]. The total charge distribution of a molecule can be used to define the MEP at a given point around it and it is connected to dipole moments. By analyzing the electron density, it can be used to determine electrophilic reactivity, nucleophilic reactivity, and hydrogen-bonding interactions [34-35]. The electrostatic potential, $V(\vec{r})$ at any point $\vec{r}$ is given by Eq. (1) [35]:

$$V(\vec{r}) = \sum_A \frac{Z_A}{|\vec{R}_A - \vec{r}|} - \int \frac{\rho(\vec{r})d\vec{r}'}{|\vec{r}' - \vec{r}|} \quad (1)$$

where $\rho(\vec{r})$ is the electronic density function molecule, Z_A is the charge on the nucleus A located at $\vec{R}_A$, and r' is the dummy integration variable. In order to predict the molecular reactive sites, the electrostatic potential surface maps have been plotted for the title compounds with B3LYP/6-311G(d,p) level shown in Fig. 3.

According to this MEP map, there are two possibilities for the electrophilic attack on the oxygen atoms (red), while the nucleophilic attack sites are located over the hydrogen atoms (yellow). These sites give information about the intermolecular interactions of our compounds. As a result, the compounds can have non-covalent interactions.

Molecular docking

Molecular docking serves as a crucial tool for investigating the optimal interaction between ligands and proteins. In our study, we employed the Pass Online tool [36] to identify promising biological activities associated with the ligands under examination, aiding us in selecting the most relevant protein targets (Table 5). Notably, HMGCS2 holds a pivotal role within the mevalonate pathway, a significant process for cholesterol synthesis. The potential to modulate HMGCS2 expression offers an innovative avenue for managing elevated cholesterol levels in cases of hypercholesterolemia. Interestingly, the ligands **2a**, **2b**, and **2c**, as indicated by Pass Online, exhibit the capacity to enhance this particular enzyme Protein PDB file was

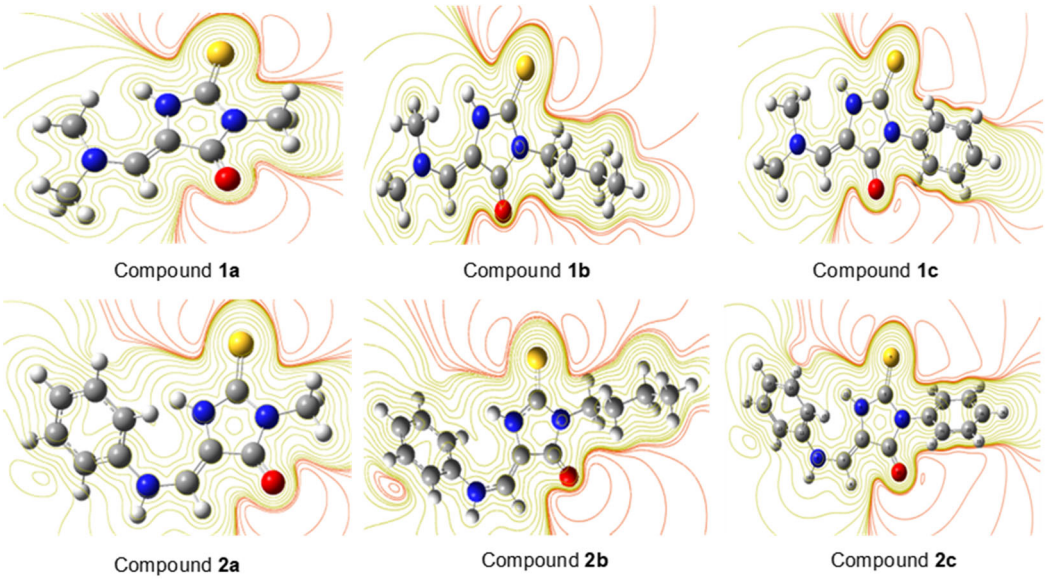

Fig 3. Molecular electrostatic potential maps calculated at B3LYP/6-311G (d,p) level

Table 5. Biological activity of ligands **2a**-**c** predicted by Pass Online

Compound **2a**			Compound **2b**			Compound **2c**		
Biological activity	PA	PI	Biological activity	PA	PI	Biological Activity	PA	PI
HMGCS2 expression enhancer	0.858	0.004	HMGCS2 expression enhancer	0.793	0.005	HMGCS2 expression enhancer	0.869	0.003
Chloride peroxidase inhibitor	0.712	0.009	Chloride peroxidase inhibitor	0.526	0.044	Chloride peroxidase inhibitor	0.740	0.007
N-methylhydantoinase (ATP-hydrolyzing) inhibitor	0.613	0.010	Antineurotic	0.563	0.085	Mcl-1 antagonist	0.672	0.005
Nicotinic α2β2 receptor antagonist	0.642	0.039	Glutaminyl-peptide cyclotransferase inhibitor	0.472	0.005	Antineoplastic (breast cancer)	0.554	0.014

downloaded from the RSCB protein database using the URL (https://www.rcsb.org/). The binding energy for ligands **2a**-**c** are listed in Table 6.

The **lig2** (**2b**) shows better binding energy to HMGCS protein, suggesting that phenyl substituent is better than methyl and butyl substituents in **lig1** (**2a**) and **lig2** (**2b**). Visualization is done on Discovery Studio [19] of **lig1** (**2a**), **lig2** (**2b**), and **lig3** (**2c**) and they are depicted in Fig. 4, 5 and 6, respectively. Despite the fact that the docking was carried out with the same active site, each ligand has interactions with different residues. In **lig1** (**2a**), Asn164 residue formed two conventional hydrogen bonds with nitrogen atoms labeled 4 and 15, exhibiting distances of 2.60 and 2.45 Å, respectively. Additionally, the phenyl substituent displayed two π-alkyl interactions with Ala165 and Lys243 residues, at distances of 4.84 and 4.14 Å, respectively. Furthermore, a carbon-hydrogen bond

Table 6. HMGCS expression enhancer predicted Pa and Pi by molecular docking

Ligand	Binding energy (kcal/mol)
lig1 (**2a**)	−6.5
lig2 (**2b**)	−6.2
lig3 (**2c**)	−7.1

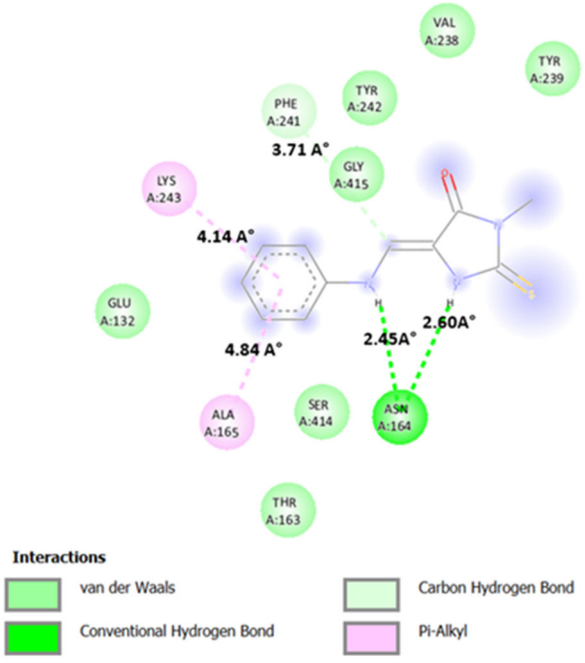

Fig 4. Molecular docking results of **lig1**-HMGCS2 complex

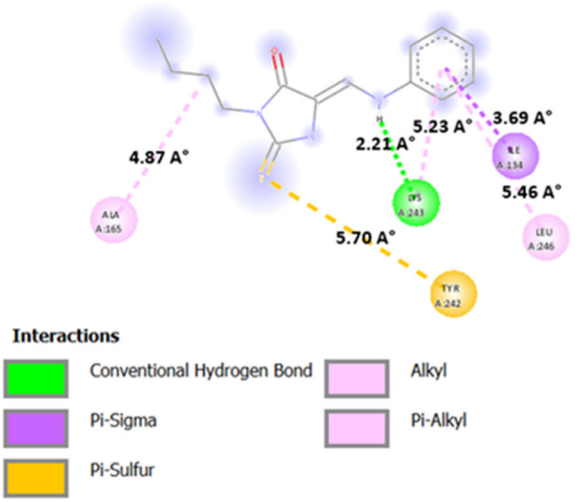

Fig 5. Molecular docking results of **lig2**-HMGCS2 complex

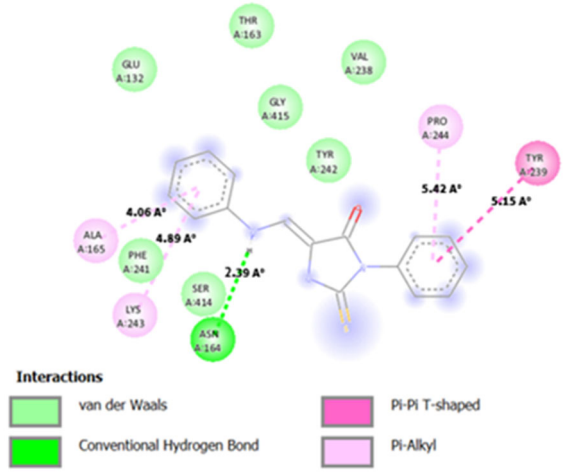

Fig 6. Molecular docking results of **lig3**-HMGCS2 complex

was observed between the carbon atom labeled 13 and Phe241 residue, with a favorable distance of 3.71 Å (Fig. 4).

In the case of **lig2** (**2b**), an alkyl interaction was established between the carbon atom labeled 27 and Ala165 residue, displaying a distance of 4.87 Å. Moreover, a pi-sulfur interaction occurred between Tyr242 and a sulfur atom labeled 7, with a distance of 5.70 Å. Lys243 residue exhibited both a conventional hydrogen bond and a π-alkyl interaction with the nitrogen atom and the phenyl group, respectively, at distances of 2.21 and 5.23 Å. Additionally, π-sigma and π-alkyl interactions were formed between the phenyl

group and residues of Ile134 and Leu246, featuring distances of 3.69 and 5.46 Å, respectively (Fig. 5).

For **lig3** (**2c**), the phenyl substituent engaged in both π-alkyl and π-π interactions with Pro244 and Tyr239, separated by distances of 5.42 and 5.15 Å, respectively. Furthermore, a conventional hydrogen bond formed between Asn164 and the nitrogen atom, with a distance of 2.39 Å. Two additional π-alkyl interactions were identified, involving the second phenyl group in the molecular structure and residues Lys243 and Ala165, with distances of 4.89 and 4.06 Å, respectively (Fig. 6).

■ CONCLUSION

In conclusion, the successful synthesis of 3-alkyl-5-phenylaminomethylene-2-thioxoimidazolidin-4-ones (**2a-c**) using microwave technology has been achieved with good yields. Structural confirmation was established through comprehensive NMR and MS spectroscopic analyses. Theoretical analysis of the electrostatic potential distribution within the compounds revealed distinct regions of electropositive and electronegative potential, aiding in the identification of donor and acceptor groups as well as charge transfer patterns and intramolecular contacts. Among the evaluated ligands, **lig2** exhibited the most favorable binding energy, indicating robust potential for meaningful interactions with the target protein. The **lig2** formed pivotal π-alkyl and π-π interactions with Pro244 and Tyr239, in conjunction with a conventional hydrogen bond involving Asn164. These interactions, coupled with the favorable binding energy, underscore the high affinity and strong molecular recognition between **lig2** and the binding site. While **lig1** displayed conventional hydrogen bonds with Asn164, along with π-alkyl interactions with Ala165 and Lys243, **lig3** demonstrated alkyl interaction with Ala165, pi-sulfur interaction with Tyr242, and both conventional hydrogen bond and π-alkyl interaction with Lys243. However, **lig2**'s superior binding energy positions it as a more promising candidate for forming a stable complex with the target protein. This highlights the potential of **lig2** as a lead compound or viable drug candidate in the realm of drug discovery and development. Continued exploration and optimization of **lig2** could further capitalize on its favorable binding attributes, potentially paving the way for enhanced therapeutic efficacy.

■ ACKNOWLEDGMENTS

This work was carried out in the Synthesis and Catalysis Laboratory (LSCT) as part of PRFU projects (code: B00L01UN140120220002) funded by the Ministry of Higher Education and Scientific Research of Algeria. We thank Prof. Óscar López (University of Seville) for his support and assistance in conducting the MS analysis and Mr. Mokhtari Zohir Abdelhak (University Ibn Khaldoun-Tiaret) for his contribution in theoretical NMR calculation.

■ AUTHOR CONTRIBUTIONS

Khedidja Merdja and Mansour Debdab wrote the paper and conducted the experiment, Mokhtaria Drissi and Farah Kaouche conducted the DFT calculations, Mustapha Rahmouni El Habib Belarbi revised the manuscript, Choukry Kamel Bendeddouche conducted the NMR experiment, Nassima Medjahed, and José Manuel Padrón conducted the MS experiment. All authors agreed to the final version of this manuscript.

■ REFERENCES

[1] Banerjee, P., Mandhare, A., and Bagalkote, V., 2022, Marine natural products as source of new drugs: An updated patent review (July 2018-July 2021), *Expert Opin. Ther. Pat.*, 32 (3), 317–363.

[2] Debdab, M., Carreaux, F., Renault, S., Soundararajan, M., Fedorov, O., Filippakopoulos, P., Lozach, O., Babault, L., Tahtouh, T., Baratte, B., Ogawa, Y., Hagiwara, M., Eisenreich, A., Rauch, U., Knapp, S., Meijer, L., and Bazureau, J.P., 2011, Leucettines, a class of potent inhibitors of cdc2-like kinases and dual specificity, tyrosine phosphorylation regulated kinases derived from the marine sponge leucettamine B: Modulation of alternative pre-RNA splicing, *J. Med. Chem.*, 54 (12), 4172–4186.

[3] Najmi, A., Javed, S.A., Al Bratty, M., and Alhazmi, H.A., 2022, Modern approaches in the discovery and development of plant-based natural products and their analogues as potential therapeutic agents,

Molecules, 27 (2), 349.

[4] Sengupta, S., Pabbaraja, S., and Mehta, G. 2023., C–H modification of natural products: A minimalist enabling tactic for drug discovery, API processing and bioconjugation, *Chem. Commun.*, 59 (62), 9445–9456.

[5] Nicolaou, K.C., and Rigol, S., 2020, Perspectives from nearly five decades of total synthesis of natural products and their analogues for biology and medicine, *Nat. Prod. Rep.*, 37 (11), 1404–1435.

[6] Debdab, M., Renault, S., Lozach, O., Meijer, L., Paquin, L., Carreaux, F., and Bazureau, J.P., 2010, Synthesis and preliminary biological evaluation of new derivatives of the marine alkaloid leucettamine B as kinase inhibitors, *Eur. J. Med. Chem.*, 45 (2), 805–810.

[7] Keel, K.L., and Tepe, J.J., 2020, The preparation of (4*H*)-imidazol-4-ones and their application in the total synthesis of natural products, *Org. Chem. Front.*, 7 (20), 3284–3311.

[8] Cho, S., Kim, S.H., and Shin, D., 2019, Recent applications of hydantoin and thiohydantoin in medicinal chemistry, *Eur. J. Med. Chem.*, 164, 517–545.

[9] de Carvalho, P.G.C., Ribeiro, J.M., Garbin, R.P.B., Nakazato, G., Yamada Ogatta, S.F., de Fátima, Â., de Lima Ferreira Bispo, M., and Macedo, F., 2020, Synthesis and antimicrobial activity of thiohydantoins obtained from L-amino acids, *Lett. Drug Des. Discovery*, 17 (1), 94–102.

[10] Li, Y., Zhang, T., Ma, H., Xu, L., Zhang, Q., He, L., Jiang, J., Zhang, Z., Zhao, Z., Wang, M., and Wang, M., 2023, Design, synthesis, and antifungal/antioomycete activity of thiohydantoin analogues containing spirocyclic butenolide, *J. Agric. Food Chem.*, 71 (16), 6249–6267.

[11] Elhady, H.A., Mohammed, S.M., Al-Shareef, H.F., and El-Mekawy, R.E., 2019, Synthesis, reactions, and applications of 2-thiohydantoin derivatives, *Acta Pol. Pharm.*, 76 (6), 971–986.

[12] Hsu, M.H., Hsieh, C.Y., Kapoor, M., Chang, J.H., Chu, H.L., Cheng, T.M., Hsu, K.C., Lin, T.E., Tsai, F.Y., and Horng, J.C., 2020, Leucettamine B analogs and their carborane derivative as potential anti-cancer agents: Design, synthesis, and biological evaluation, *Bioorg. Chem.*, 98, 103729.

[13] Khodair, A.I., El-Barbary, A.A., Imam, D.R., Kheder, N.A., Elmalki, F., and Ben Hadda, T., 2021, Synthesis, antiviral, DFT and molecular docking studies of some novel 1,2,4-triazine nucleosides as potential bioactive compounds, *Carbohydr. Res.*, 500, 108246.

[14] Bendeddouche, C.K., Adjdir, M., and Benhaoua, H., 2016, Stereoselective cyclopropanation under solvent free conditions: Catalyzed by a green and efficient recyclable Cu-exchanged bentonite, *Lett. Org. Chem.*, 13 (3), 217–223.

[15] Bendeddouche, S., Bendeddouche, C.K., and Benhaoua, H., 2021, A Convenient stereoselective method for synthesis of β-lactams under microwave irradiation with [BmIm] OH as a reusable ionic liquid, *Lett. Org. Chem.*, 18 (12), 929–935.

[16] Chérouvrier, J.R., Carreaux, F., and Bazureau, J.P., 2002, A practical and eco-friendly synthesis of stereo controlled alkylaminomethylidene derivatives of 2-thiohydantoins by dimethylamine substitution, *Tetrahedron Lett.*, 43 (48), 8745–8749.

[17] Kourat, O., Djafri, A., Benhalima, N., Megrouss, Y., Belkafouf, N.E.H., Rahmani, R., Daran, J.C., Djafri, A., and Chouaih, A., 2020, Synthesis, crystal structure, Hirshfeld surface analysis, spectral characterization, reduced density gradient and nonlinear optical investigation on (*E*)-*N*'-(4-nitro benzylidene)-2-(quinolin-8-yloxy) acetohydrazide monohydrate: A combined experimental and DFT approach, *J. Mol. Struct.*, 1222, 128952.

[18] Metwally, M.A., and Abdel-Latif, E., 2012, Thiohydantoins: Synthetic strategies and chemical reactions, *J. Sulfur Chem.*, 33 (2), 229–257.

[19] Osyanin, V.A., Korzhenko, K.S., Rashchepkina, D.A., Osipov, D.V., and Klimochkin, Y.N., 2021, Nucleophilic vinylic substitution in perfluoroacylchromenes. Diastereoselective synthesis of push–pull enamino ketones, *Russ. J. Org. Chem.*, 57 (7), 1053–1062.

[20] Frisch, M.J., Trucks, G.W., Schlegel, H.B., Scuseria, G.E., Robb, M.A., Cheeseman, J.R., Scalmani, G.,

Barone, V., Mennucci, B., Petersson, G.A., Nakatsuji, H., Caricato, M., Li, X., Hratchian, H.P., Izmaylov, A.F., Bloino, J., Zheng, G., Sonnenberg, J.L., Hada, M., Ehara, M., Toyota, K., Fukuda, R., Hasegawa, J., Ishida, M., Nakajima, T., Honda, Y., Kitao, O., Nakai, H., Vreven, T., Montgomery, Jr., J.A., Peralta, J.E., Ogliaro, F., Bearpark, M., Heyd, J.J., Brothers, E., Kudin, K.N., Staroverov, V.N., Kobayashi, R., Normand, J., Raghavachari, K., Rendell, A., Burant, J.C., Iyengar, S.S., Tomasi, J., Cossi, M., Rega, N., Millam, J.M., Klene, M., Knox, J.E., Cross, J.B., Bakken, V., Adamo, C., Jaramillo, J., Gomperts, R., Stratmann, R.E., Yazyev, O., Austin, A.J., Cammi, R., Pomelli, C., Ochterski, J.W., Martin, R.L., Morokuma, K., Zakrzewski, V.G., Voth, G.A., Salvador, P., Dannenberg, J.J., Dapprich, S., Daniels, A.D., Farkas, O., Foresman, J.B., Ortiz, J.V., Cioslowski, J., and Fox, D.J., 2009, *Gaussian 09, Revision A.02*, Gaussian, Inc., Wallingford CT.

[21] Dennington, R., Keith, T.A., and Millam, J.M., 2009, *GaussView*, Version 5, Semichem Inc., Shawnee Mission, KS.

[22] Raczyńska, E.D., Gal, J.F., Maria, P.C., Sakhawat, G.S., Fahim, M.Q., and Saeidian, H., 2022, Nitriles with high gas-phase basicity—Part II Transmission of the push–pull effect through methylenecyclopropene and cyclopropenimine scaffolds intercalated between different electron donor(s) and the cyano *N*-protonation site, *Molecules*, 27 (14), 4370.

[23] Eberhardt, J., Santos-Martins, D., Tillack, A Forli, S., 2021, AutoDock Vina 1.2.0: New docking methods, expanded force field, and python bindings, *J. Chem. Inf. Model.*, 61 (8), 3891–3898.

[24] Boukabcha, N., Direm, A., Drissi, M., Megrouss, Y., Khelloul, N., Dege, N., Tuna, M., and Chouaih, A., 2021, Synthesis, structural determination, Hirshfeld surface analysis, 3D energy frameworks, electronic and (static, dynamic) NLO properties of *o*-Nitroacetanilide (*o*-NAA): A combined experimental and quantum chemical study, *Inorg. Chem. Commun.*, 133, 108884.

[25] Mollaamin, F., and Monajjemi, M., 2023, Molecular modelling framework of metal-organic clusters for conserving surfaces: Langmuir sorption through the TD-DFT/ONIOM approach, *Mol. Simul.*, 49 (4), 365–376.

[26] Suresh, C.H., Remya, G.S., and Anjalikrishna, P.K., 2022, Molecular electrostatic potential analysis: A powerful tool to interpret and predict chemical reactivity, *WIREs Comput. Mol. Sci.*, 12 (5), e1601.

[27] Nehra, N., Tittal, R.K., and Ghule, V.D., 2021, 1,2,3-Triazoles of 8-hydroxyquinoline and HBT: Synthesis and studies (DNA binding, antimicrobial, molecular docking, ADME, and DFT), *ACS Omega*, 6 (41), 27089–27100.

[28] Singh, J.S., Khan, M.S., and Uddin, S., 2023, A DFT study of vibrational spectra of 5-chlorouracil with molecular structure, HOMO–LUMO, MEPs/ESPs and thermodynamic properties, *Polym. Bull.*, 80 (3), 3055–3083.

[29] Li, D.D., and Greenfield, M.L., 2014, Chemical compositions of improved model asphalt systems for molecular simulations, *Fuel*, 115, 347–356.

[30] Mulliken, R.S., 1962, Criteria for the construction of good self-consistent-field molecular orbital wave functions, and the significance of lCAO-MO population analysis, *J. Chem. Phys.*, 36 (12), 3428–3439.

[31] Rigby, J., and Izgorodina, E.I., 2013, Assessment of atomic partial charge schemes for polarisation and charge transfer effects in ionic liquids, *Phys. Chem. Chem. Phys.*, 15 (5), 1632–1646.

[32] Drissi, M., Benhalima, N., Megrouss, Y., Rachida, R., Chouaih, A., and Hamzaoui, F., 2015, Theoretical and experimental electrostatic potential around the m-nitrophenol molecule, *Molecules*, 20 (3), 4042–4054.

[33] Abraham, C.S., Prasana, J.C., Muthu, S., Rizwana B, F., and Raja, M., 2018, Quantum computational studies, spectroscopic (FT-IR, FT-Raman and UV–Vis) profiling, natural hybrid orbital and molecular docking analysis on 2,4 Dibromoaniline, *J. Mol. Struct.*, 1160, 393–405.

[34] Guediri, A., Bouguettoucha, A., Chebli, D., Chafai, N., and Amrane, A., 2020, Molecular dynamic simulation and DFT computational studies on the

adsorption performances of methylene blue in aqueous solutions by orange peel-modified phosphoric acid, *J. Mol. Struct.*, 1202, 127290.

[35] Politzer, P., and Murray, J.S., 2021, Electrostatic potentials at the nuclei of atoms and molecules, *Theor. Chem. Acc.*, 140 (1), 7.

[36] Filimonov, D.A., Lagunin, A.A., Gloriozova, T.A., Rudik, A.V., Druzhilovskii, D.S., Pogodin, P.V., and Poroikov, V.V., 2014, Prediction of the biological activity spectra of organic compounds using the PASS online web resource, *Chem. Heterocycl. Compd.*, 50 (3), 444–457.